Seventh Mississippi State - UAB Conference on Differential Equations and Computational Simulations, *Electronic Journal of Differential Equations*, Conference 17 (2009), pp. 1–11.
ISSN: 1072-6691. URL: http://ejde.math.txstate.edu or http://ejde.math.unt.edu
ftp ejde.math.txstate.edu

METHANE HYDRATE FORMATION AND DECOMPOSITION

VASILIOS ALEXIADES

Abstract. Methane hydrates, in arctic permafrost and deep ocean sediments, store vast amounts of methane, which is the primary constituent of natural gas and a potent greenhouse gas.

Methane hydrate is a crystaline solid consisting of methane surrounded by frozen water molecules. It is stable in a narrow range of high pressures and low temperatures. Thus, issues affecting the stability of hydrate layers and phase change processes that may disturb this stability are of utmost importance.

We present simulations with an isobaric compositional thermal model, based on conservation laws for species and energy, which allows composition, temperature, and pressure dependence of material properties, with thermodynamically consistent treatment of phase behavior via equations of state.

1. Introduction

Methane hydrate is ice that burns! (Fig. 1). It is a crystalline compound of methane and water, stable under a narrow zone of low temperatures and high pressures. The *Structure I hydrate* consists of 46 water molecules per 8 gas molecules, forming two small dodecahedral and six large tetrakaidecahedral cavities into which methane molecules enter and stabilize the structure (Fig. 2a).

Its mean radius is about 12 angstroms and its theoretical composition is 8:46 = 14.8% CH_4. The structure packs a great amount of methane; a liter of *pure* methane hydrate releases 164 liters of gas!

Methane hydrates are found in sandy sediments at the bottom of oceans all around the margins of continents at great depths of 300–3000 m, at temperatures of 0–20 °C (Fig. 2b), and under permafrost in arctic regions. A liter of sediment yields 10 to 50 liters of methane gas. Thus, methane hydrate deposits constitute a potentially enormous natural gas resource, if the gas could be extracted safely and economically. On the other hand, methane being a potent green house gas, it is feared that global warming may destabilize methane hydrate deposits and release vast amounts of methane to the atmosphere. Thus, issues of formation/dissociation

2000 *Mathematics Subject Classification.* 92C45, 35K60, 65M99.
Key words and phrases. Phase change; enthalpy; heat conduction; diffusion; thermochemistry; gas hydrates; finite volume scheme.
©2009 Texas State University - San Marcos.
Published April 15, 2009.

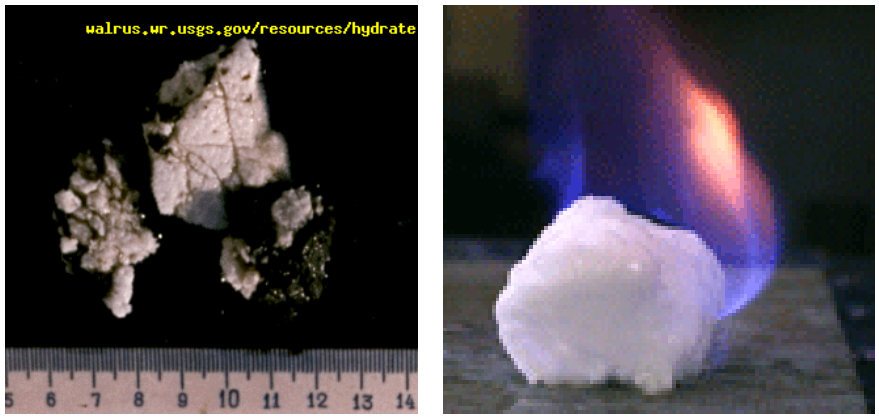

FIGURE 1. Ice that burns!

and (thermodynamic) stability of hydrates are of utmost concern and need to be studied via experiments and modeling.

Primary references on gas hydrates are the books by Makogon [2] and by Sloan [4], while the research literature is expanding rapidly, see e.g. [6]. The current state of hydrate research efforts in the USA can be found in [3].

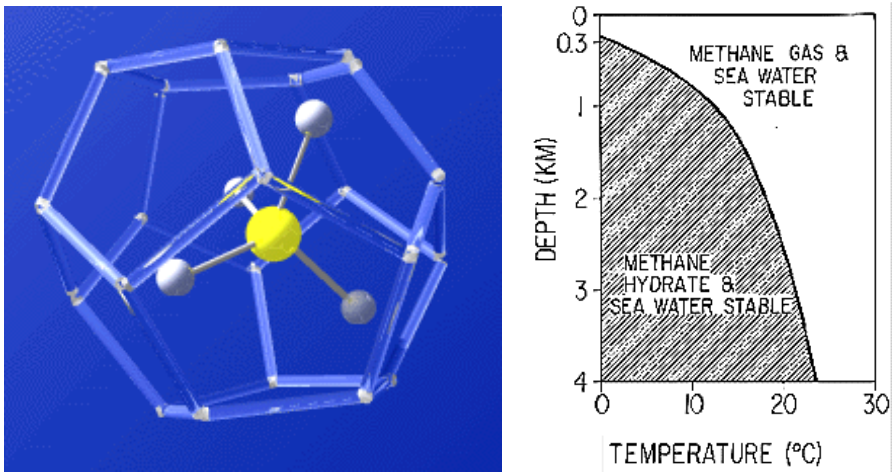

FIGURE 2. Methane hydrate crystaline structure (left), and temperature-depth stability region (right). From [7].

As a first step in understanding such issues, we present a mathematical model of hydrate formation/decomposition under constant pressure (isobaric) that incorporates compositional and thermal effects, consistent with the thermochemistry of phases as dictated by the composition - temperature phase diagram of the water–methane binary system $(H_2O)_{1-x}(CH_4)_x$, with x the mole fraction of methane.

2. Isobaric Compositional-Thermal Model

At a typical pressure of 4.8 MPa, corresponding to a depth of 470 m (for which the phase diagram is known, [4]), the water–methane binary $(H_2O)_{1-x}(CH_4)_x$ can form three primary stable phases, (Fig. 3) which we label as:

$$\begin{aligned} \mathbf{LG} &= \textit{Liquid water + methane Gas}, \\ \mathbf{SL} &= \textit{Solid hydrate + Liquid water}, \\ \mathbf{SG} &= \textit{Solid hydrate + methane Gas}. \end{aligned}$$

At temperature $T_E = 6.285°$C, the three phases coexist. Above T_E, water and gas mix at all proportions (except very near $x = 0$ and $x = 1$, shown exaggerated in Fig. 3)). For $0°\text{C} \le T \le T_E$ and $x < x_E = 8/54 = 14.8\%$ we find SL (hydrate+water), whereas for $x > x_E$ we find SG (hydrate+gas).

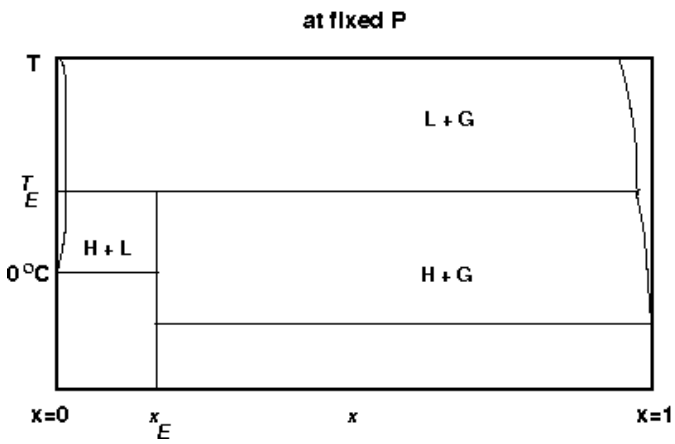

Figure 3. Methane hydrate phase diagram (schematic) at 4.8 MPa, around the 3-phase coexistence line at $T_E = 6.285°C$.

Employing conservation laws for species and energy, the $x - T$ phase diagram, and Equations of State (EoS) developed below, we seek to determine x, T, and the mole fractions λ^L, λ^S, λ^G of liquid(L), hydrate(S), gas(G), as they evolve in space and time from given initial and boundary conditions.

2.1. Conservation laws (for constant P, ρ).

Denoting the species as $A = H_2O$, $B = CH_4$, and their molecular weights by W_A, W_B, the formula molecular weight for the binary $A_{1-x}B_x$ is $W(x)=(1-x)W_A + xW_B$. The mass fraction of methane, corresponding to mole fraction x, is $w \equiv w_B = xW_B/W(x)$, and that of water is $w_A=(1-x)W_A/W(x)$ since $w_A + w_B=1$. Conversely, knowing w, we can find the mole fraction $x \equiv x_B = wW_A/[wW_A+(1-w)W_B]$. Thus, either x or w can be used as composition variable, and one can be found from the other. Thermochemistry uses x=mole fraction, but we prefer to express conservation laws in terms of w=weight fraction, as is commonly done.

Under the assumptions of constant pressure and constant density=ρ, letting H=molar enthalpy and $h=H/W(x)$=enthalpy (per gram), conservation of species B (methane) and energy (enthalpy) are expressed as:

$$\partial_t(\rho w) + \nabla \cdot \vec{J}_B = 0, \qquad \partial_t(\rho h) + \nabla \cdot \vec{Q} = 0, \tag{2.1}$$

with mass flux $\vec{J}_B = -\rho D \nabla w$, and heat flux $\vec{Q}$ given by

$$\vec{Q} = -k\nabla T + \overline{h}_A \vec{J}_A + \overline{h}_B \vec{J}_B \ = -k\nabla T + \overline{h}\vec{J}_B, \quad with \overline{h} = \overline{h}_B - \overline{h}_A. \tag{2.2}$$

Here D=diffusivity of methane in water, k=thermal conductivity, and $\overline{h}_i$=partial enthalpy of species $i = A, B$. Note that $w_A = 1 - w$ and $\vec{J}_A = -\vec{J}_B$, so A is also conserved.

The conservation laws are valid mathematically, in weak sense, throughout the system, irrespective of phase (with coefficients appropriate to phase: k^{LG}, k^{SL}, k^{SG}, $\overline{h}^{LG}$, $\overline{h}^{SL}$, $\overline{h}^{SG}$, etc). The conservation laws update ρw and ρh to new time, from which we find w and h, and therefore x and H as above. Then, to find the new phase, temperature, and phase fractions, we need Equations of State $H = H(x, T, P)$ consistent with the phase diagram (Fig. 3), which we now develop.

2.2. **Equations of State.** Choose the reference state to be *hydrate* at $(x_E, T_E(P))$ with reference enthalpy H_E. The enthalpy in each phase (LG , SL, SG) can be expressed in terms of the pair (x, T) by integration, along constant x and constant T paths on the phase diagram, of the basic Gibbs relation

$$dH^\alpha = \overline{H}^\alpha dx + C_p^\alpha dT \quad \alpha = \text{LG, SL, SG}, \tag{2.3}$$

where $\overline{H}^\alpha$=$\overline{H}_B^\alpha - \overline{H}_A^\alpha$, C_p^α=heat capacity of phase α = LG, SL, SG.

We obtain the following EoS for H in terms of (x, T):

• In **LG** (for $T \geq T_E$, $0 \leq x \leq 1$):

$$H^{LG}(x,T) = \mathrm{H}^{\mathbf{L}}(x) + \int_{T_E}^{T} C_p^{LG}(x,\tau)d\tau,$$
$$\text{where} \quad \mathrm{H}^{\mathbf{L}}(x) := H_E + \Delta H_E^{fus} + \int_{x_E}^{x} \overline{H}^{LG}(\xi, T_E)d\xi.$$

• In **SL** (for $T < T_E$, $0 \leq x \leq x_E$):

$$H^{SL}(x,T) = \mathrm{H}^{\mathbf{S}}(x) - \int_{T}^{T_E} C_p^{SL}(x,\tau)d\tau,$$
$$\text{where} \quad \mathrm{H}^{\mathbf{S}}(x) := H_E + \int_{x_E}^{x} \overline{H}^{SL}(\xi, T_E)d\xi.$$

• In **SG** (for $T < T_E$, $x_E \leq x \leq 1$):

$$H^{SG}(x,T) = \mathrm{H}^{\mathbf{S}}(x) - \int_{T}^{T_E} C_p^{SG}(x,\tau)d\tau,$$
$$\text{where} \quad \mathrm{H}^{\mathbf{G}}(x) := H_E + \int_{x_E}^{x} \overline{H}^{SG}(\xi, T_E)d\xi.$$

Since the heat capacity is strictly positive, the dependence of H on T is monotonic, so T can be found from H. Moreover, the quantities $\mathrm{H}^{\mathbf{L}}(x), \mathrm{H}^{\mathbf{S}}(x), \mathrm{H}^{\mathbf{G}}(x)$ can be used as switches to distinguish the phases. Thus, the phases are equally well characterized by the pair (x, H) as follows:

• If $H \geq \mathbf{H}^{\mathbf{L}}(x)$ then phase is **LG**:
find T $(\geq T_E)$ by solving the EoS $\int_{T_E}^{T} C_p^{LG}(x,\tau)d\tau = H - \mathrm{H}^{\mathbf{L}}(x) \quad (\geq 0)$ for T, and then the phase fractions are:

$$\lambda^L = \tfrac{x^G(T)-x}{x^G(T)-x^L(T)}, \quad \lambda^G = 1 - \lambda^L, \qquad \lambda^S = 0.$$

Otherwise, the phase depends on the value of x:

• For $x < x_E$, if $H < \mathbf{H}^{\mathbf{S}}(x)$, then phase is **SL**
find T $(< T_E)$ by solving the EoS $\int_{T}^{T_E} C_p^{SL}(x,\tau)d\tau = H - \mathrm{H}^{\mathbf{S}}(x) \quad (< 0)$ for T, and then the phase fractions are:

$$\lambda^S = \tfrac{x-x^L(T)}{x^S(T)-x^L(T)}, \quad \lambda^L = 1 - \lambda^S, \quad \lambda^G = 0, \quad \text{if } x < x_E,$$

- For $x > x_E$, if $H < \mathbf{H^G}(x)$, then phase is **SG**
  find T ($< T_E$) by solving the EoS $\int_T^{T_E} C_p^{SG}(x,\tau)d\tau = H - \mathrm{H}^{\mathbf{G}}(x) \quad (< 0)$ for T, and then the phase fractions are:
  $$\lambda^S = \tfrac{x^G(T)-x}{x^G(T)-x^S(T)}, \quad \lambda^G = 1-\lambda^S \quad \lambda^L = 0, \quad \text{if } x > x_E.$$
- **Otherwise, three-phase L+S+G**, so $T = T_E$,
  and phase fractions are found from the relations:
  $\lambda^L x^L + \lambda^S x^S + \lambda^G x^G = x, \quad \lambda^L H^L + \lambda^S H^S + \lambda^G H^G = H, \quad \lambda^L + \lambda^S + \lambda^G = 1.$

The PDEs are discretized by finite volumes, and explicitly in time. The enthalpy algorithm proceeds as follows: Knowing the current values of T and phase fractions, we evaluate the property values, compute the fluxes $\vec{J}$, $\vec{Q}$, and update ρw, ρh from the PDEs. From w and h we find x, H and the phase indicators $\mathrm{H}^{\mathbf{L}}(x)$, $\mathrm{H}^{\mathbf{S}}(x)$, $\mathrm{H}^{\mathbf{G}}(x)$, which determine the temperature and phase fractions as just described.

The model needs the following thermophysical data (as functions of x, T): thermal conductivities k^S, k^L, k^G, diffusivities (of methane) D^S, D^L, D^G, partial enthalpies $\overline{H}_i^S$, $\overline{H}_i^L$, $\overline{H}_i^G$, of species i=water, methane, heat of fusion (latent heat) ΔH^{fus}, and the $x-T$ phase diagram (at the desired pressure). Some of these quantities were obtained/adapted from the literature ([2], [4], [1], [8]), some from phase-equilibria software ([5]), and some were derived as ideal mixtures of their components. We do not present them here are they are rather involved and messy. In addition, simulation of heat transfer in the container walls requires the density, conductivity, and specific heat of the wall material, which are constants over our short temperature range of interest (1 - 25°C).

3. Numerical Simulations

We simulate methane hydrate formation and decomposition in a cylindrical steel pressure vessel (Fig. 4) of inner radius 16 and height 91 cm, with wall thickness 2.2 cm laterally and 14.6 cm at top and bottom. The vessel is filled up to height of 64 cm, the rest is water vapor. In the axially-symmetric simulations, in (r, z) coordinates, a rather coarse mesh of 32 radial and 128 axial nodes was used (roughly 0.5 by 0.5 cm), and 32 by 16 nodes in the void (plus 4 radial and 2×14 axial nodes in the wall), for a total of $36 \times 172 = 6192$ control volumes. This is adequate for the scoping studies presented here as finer meshes did not make noticeable difference in the results. A typical simulation takes about 5 minutes (on an AMD Opteron 252, 2.6 GHz processor).

We present (axi-symmetric) simulations for four scenarios below. In the two hydrate formation studies (§3.1-3.2) we start at a uniform temperature $T_{init} = 25°\mathrm{C}$ and cool the system by imposing $T_{bry} = 1°\mathrm{C}$ at the outer surface of the vessel. Conversely, in the two hydrate decomposition studies (§3.3-3.4) we start at $T_{init} = 1°\mathrm{C}$ and heat the vessel to $T_{bry} = 25°\mathrm{C}$. Contour plots for temperature and phase fractions are shown in the region occupied by the phase-change material (water–methane), namely for $0 \le r \le 16\,\mathrm{cm}$ and $0 \le z \le 64\,\mathrm{cm}$ (with z increasing downwards, representing depth).

3.1. Hydrate Formation.

We start with a water+methane mixture at composition $x = 0.1$ (that is, 90% water - 10% methane) and temperature $T_{init} = 25°\mathrm{C}$. According to the phase diagram the system is in the **LG** phase. We impose $T_{bry} = 1°\mathrm{C}$ on the outer surface of the vessel. Fig. 5 displays contours of temperature and of the gas, liquid, and solid fractions at 6 hours. Temperature history at three heights

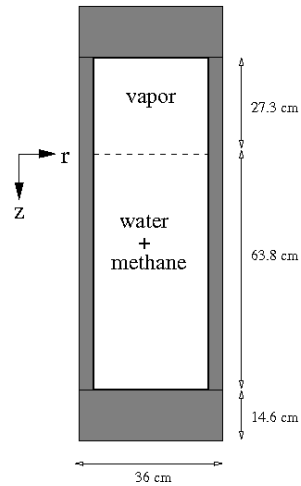

FIGURE 4. Pressure vessel (schematic).

(bottom, middle, top, at half-radius), and radial profiles at 6 and 36 hours are seen in Fig. 6. The bottom cools most rapidly and the middle the slowest, as expected. Complete cooling to $\sim 1°$C occurs in about 84 hours, while the phase fractions relax to essentially uniform values by 78 hours. The result is 70% solid (hydrate) and 30% liquid (water).

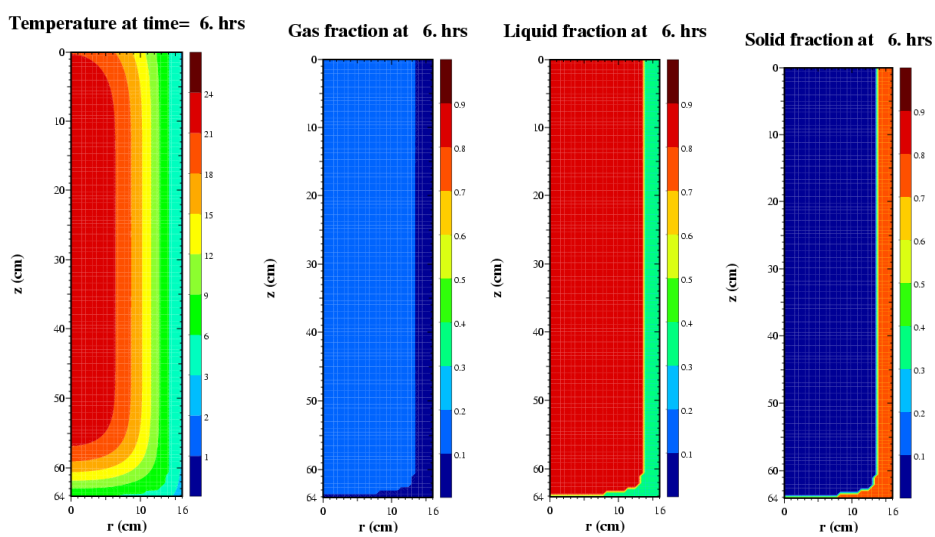

FIGURE 5. Formation (see §3.1): Contour plots of T and phase fractions $\lambda^G, \lambda^L, \lambda^S$ at 6 hours.

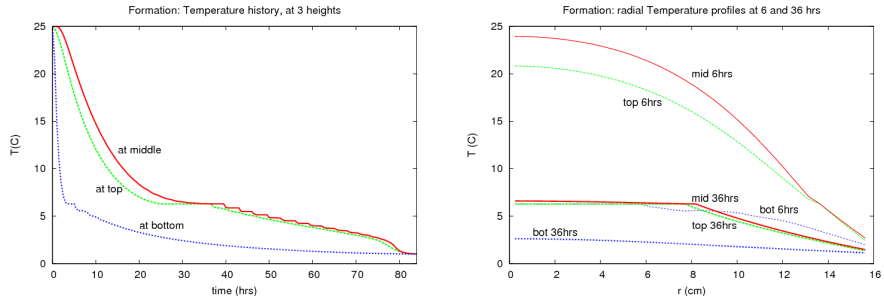

FIGURE 6. Formation (see §3.1): Temperature history at three heights (left). Radial profiles at 6 and 36 hours (right).

3.2. **Hydrate Formation with gas bubble.** Now we start again in the **LG** phase at $x = 0.1$, $T_{init} = 25°\text{C}$ and impose $T_{bry} = 1°\text{C}$, but we assume there is a pre-existing methane gas bubble ($\lambda^G = 1$, $\lambda^L = \lambda^S = 0$) at the center. Contour plots of temperature and of the phase fractions at 6 hours are shown in Fig. 7.

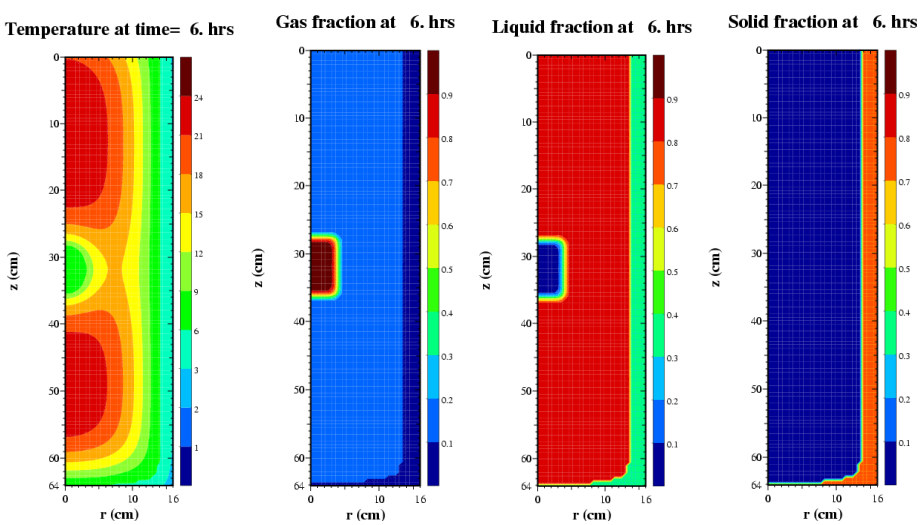

FIGURE 7. Formation with gas bubble at the center initially (see §3.2). Contour plots of T and $\lambda^G, \lambda^L, \lambda^S$ at 6 hours.

Complete cooling to nearly 1°C again takes about 84 hours, but now the phase fractions do not relax to their final uniform values till much much later. Even after 240 hours there are non-uniformities, shown in Fig. 8, revealing higher hydrate fraction around the pre-existing gas bubble. It persists for a very long time after temperature gradients have dissipated, due to the very low diffusivity of methane. The final result is again 70% hydrate and 30% water.

3.3. **Hydrate Decomposition.** Here we start in the **SL** phase with hydrate+water at $x = 0.1$, at a cold temperature $T_{init} = 1°\text{C}$ and impose $T_{bry} = 25°\text{C}$ on the outer surface of the vessel. Contours of temperature and of the gas, liquid, and solid

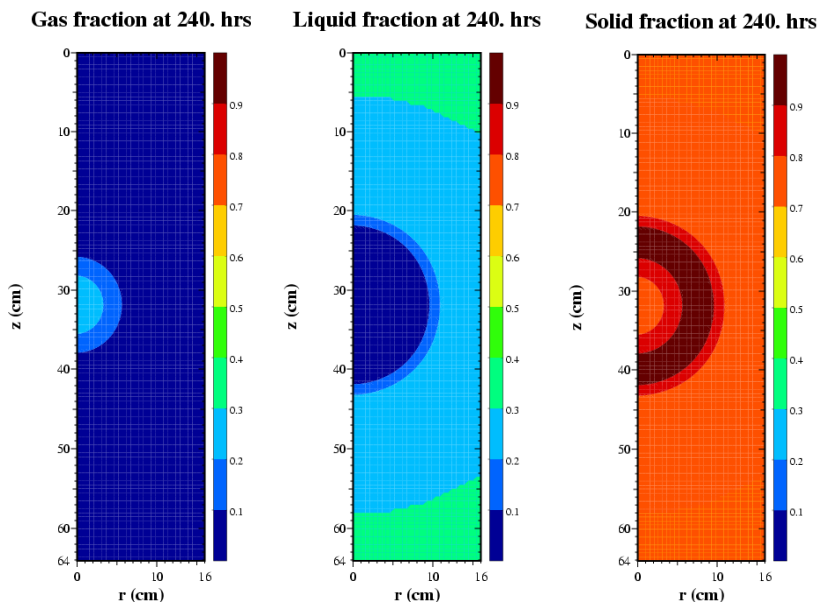

FIGURE 8. Formation with gas bubble at the center initially (see §3.2). The persisting phase fractions $\lambda^G, \lambda^L, \lambda^S$ at 240 hours.

fractions at 24 hours are shown in Fig. 9. Complete warming to nearly 25°C takes about 168 hours, much longer than the corresponding formation case of §3.1. The result is 89% liquid (water) and 11% gas (methane).

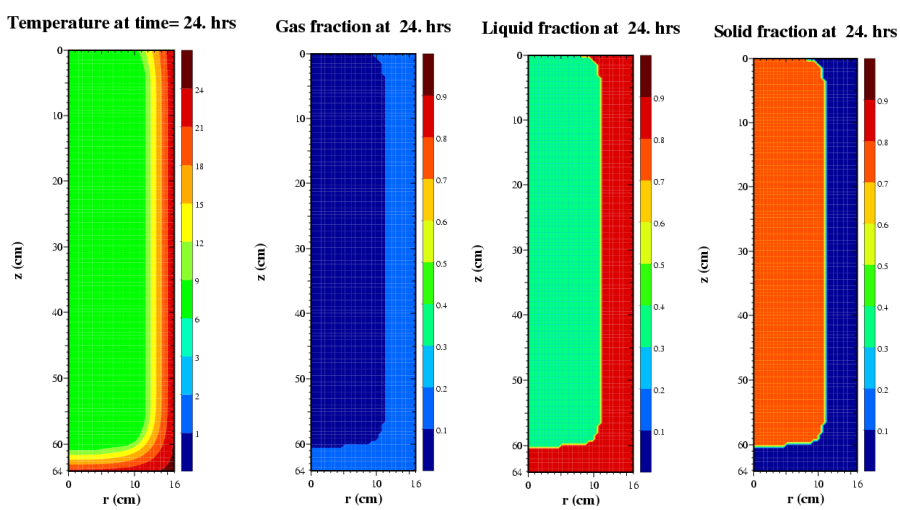

FIGURE 9. Decomposition (§3.3): Contour plots of temperature and $\lambda^G, \lambda^L, \lambda^S$ at 24 hours.

3.4. **Hydrate Decomposition with gas bubble.** In this simulation, we start again in the **SL** phase at $x = 0.1$, $T_{init} = 1$°C and impose $T_{bry} = 25$°C, but

now we assume there is an all-gas bubble ($\lambda^G = 1$, $\lambda^S = \lambda^L = 0$) at the center. Complete heating to nearly 25°C takes about 160 hours, but the evolution of the phase fractions is quite different, shown in Fig. 10 at 24 hours.

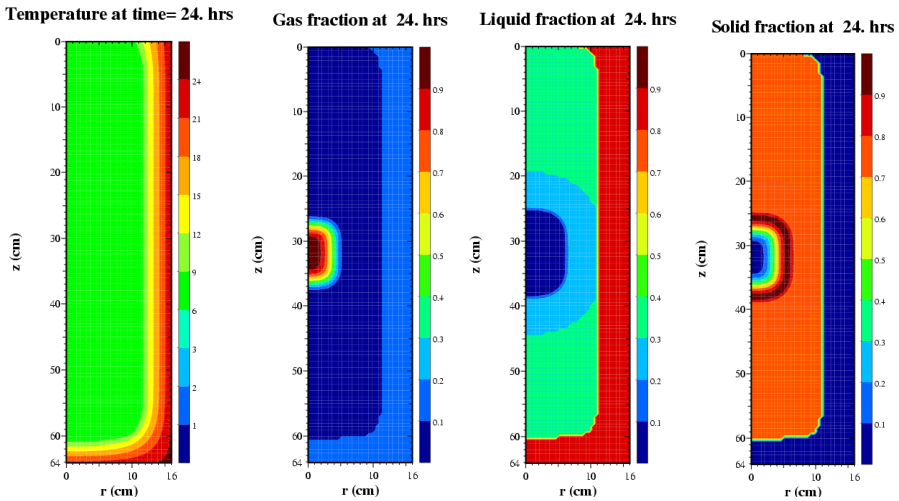

FIGURE 10. Decomposition with gas bubble at the center (§3.4). Contour plots of temperature and $\lambda^G, \lambda^L, \lambda^S$ at 24 hours.

The solid phase disappears by 132 hours, but the liquid and gas fractions take a very long time to relax to uniform values, seen at 240 hours in Fig. 11. The ultimate result is again 89% water and 11% gas.

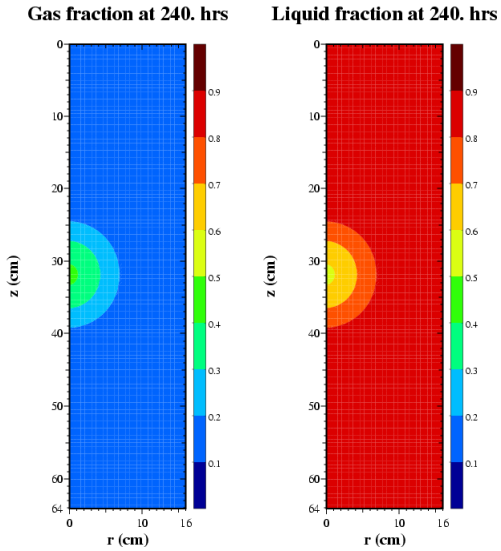

FIGURE 11. Decomposition with gas bubble at the center (§3.4). Persisting λ^G and λ^L at 240 hours.

4. Discussion

An isobaric conduction-diffusion model for hydrate formation and decomposition was presented, based on species and energy conservation laws, and Equations of State consistent with thermochemistry and the phase diagram of the water–methane binary system $(H_2O)_{1-x}(CH_4)_x$. Given the initial composition x, temperature T_{init}, and imposed temperature T_{bry} on the outer surface of the vessel, the model tracks x, T, and the phase fractions $\lambda^G, \lambda^L, \lambda^S$ of gas (methane), liquid (water), solid (hydrate), as they evolve in space and time.

Axially-symmetric numerical simulations in a cylindrical pressure vessel were carried out to find out basic features of hydrate formation and decomposition processes. These include how long the process takes (for gradients to dissipate), and the final phase fractions produced.

Sample simulations were presented in §3 for composition $x = 0.1$. The behavior is similar for other compositions we have tested ($x = 0.15, 0.2, 0.4, 0.5, 0.8, 0.9$) under conditions identical to those in §3.1 (for formation) and §3.3 (for decomposition). Pertinent resuls are summarized in the tables below.

Table 1 shows how long it takes for a formation or decomposition process to complete for various compositions. Decomposition is much slower than formation (as already noted in §3.3), except in the $x = 0.8$ case in which the gas content is very high.

Table 1. Number of hours for each quantity to roughly equilibrate to its final value, for formation (§3.1) and decomposition (§3.3) for various initial compositions x.

	Formation		Decomposition	
x	T°C	λ^G,λ^L,λ^S $\tilde{}$(%)	T°C	λ^G,λ^L,λ^S $\tilde{}$(%)
0.10	84	78	168	132
0.15	66	66	162	132
0.20	66	66	162	132
0.50	96	90	162	132
0.80	170	166	148	132

Finally, in Table 2 we list the initial and final percentage of phases, for various compositions x, in the case of formation (cooling from 25°C down to 1°C), and of decomposition (heating from 1°C up to 25°C).

We observe that for each composition x one process undoes the effect of the other, recycling the system back to its original state (under the ideal conditions assumed here). E.g. formation for $x = 0.2$ starts with $\lambda^G = 21\%$, $\lambda^L = 79\%$ and produces $\lambda^G = 7\%$, $\lambda^S = 93\%$. Conversely, decomposition for $x = 0.2$ starts with $\lambda^G = 7\%$, $\lambda^S = 93\%$ and produces $\lambda^G = 21\%$, $\lambda^L = 79\%$.

The maximum amount of hydrate is obtained for composition $x = 0.15$, as dictated by the phase diagram, because $x = 0.15$ is very close to the theoretical ratio $x_E = 8 : 46 \approx 0.148$ of hydrate formation.

The model can be used to study sensitivity of parameters and uncertainty quantification, and towards determining unavailable thermophysical parameters. For

Table 2. Initial and final phase fractions (expressed in %)

	initial values (%)			final values (%)		
x	λ^G	λ^L	λ^S	λ^G	λ^L	λ^S
Formation						
0.10	11	89	-	0	30	70
0.15	16	84	-	1	0	99
0.20	21	79	-	7	0	93
0.50	54	46	-	42	0	58
0.80	86	14	-	77	0	23
Decomposition						
0.10	-	30	70	11	89	0
0.15	1	-	99	16	84	0
0.20	7	-	93	21	79	0
0.50	42	-	58	54	46	0
0.80	77	-	23	86	14	0

increasing realism, the model can be enhanced by incorporating effects of salinity, of crystallization and decomposition kinetics, of sediments, and ultimately also of microbiological activity as a source of methane in sediments.

References

[1] V Alexiades and A D Solomon **Mathematical Modeling of Melting and Freezing Processes**, Hemisphere Publ.Co., 1993.

[2] Yuri F Makogon, **Hydrates of Hydrocarbons**, Pennwell Books, 1997.

[3] National Methane Hydrate R&D Program, http://www.netl.doe.gov/technologies/oil-gas/futuresupply/methanehydrates/maincontent.htm (accessed September 2008).

[4] E Dendy Sloan, Jr., **Clathrate Hydrates of Natural Gases**, 2nd Ed., Marcel Dekker, 1998.

[5] W Wagner, EQTEST (fortran code) for thermodynamic properties of H2O and of CH4, Ruhr-Universitt Bochum, 1995.

[6] Joseph W Wilder, et.al., "An International Effort to Compare Gas Hydrate Reservoir Simulators" Proceedings of 6th International Conference on Gas Hydrates (ICGH 2008), Vancouver, CANADA, July 6-10, 2008. http://www.netl.doe.gov/technologies/oil-gas/FutureSupply/MethaneHydrates/MH_CodeCompare/MH_CodeCompare.html (accessed September 2008).

[7] Woods Hole Science Center http://woodshole.er.usgs.gov/project-pages/hydrates/what.html (accessed September 2008).

[8] O.Y. Zatsepina and B.A. Buffett, "Phase equilibrium of gas hydrate: implications for the formation of hydrate in the deep sea floor", *Geophys. Res. Lett.* **24**: 1567-1570, 1997

Vasilios Alexiades

Department of Mathematics, University of Tennessee, Knoxville, TN 37996, USA and Oak Ridge National Laboratory, Oak Ridge TN 37831, USA

E-mail address: alexiades@utk.edu